Self-Assembled Monolayer-Functionalized Half-Metallic Manganite for Molecular Spintronics

Sergio Tatay,[†,*] Clément Barraud,[†] Marta Galbiati,[†] Pierre Seneor,[†,*] Richard Mattana,[†,*] Karim Bouzehouane,[†] Cyrile Deranlot,[†] Eric Jacquet,[†] Alicia Forment-Aliaga,[‡] Pascale Jegou,[§] Albert Fert,[†] and Frédéric Petroff[†]

[†]Unité Mixte de Physique CNRS/Thales, 1 Avenue Auguste Fresnel, 91767 Palaiseau, and Université Paris-Sud, 91405 Orsay, France, [‡]Institute for Molecular Science, University of Valencia, C/ Catedrático José Beltrán 2, E-46980, Paterna, Spain, and [§]CEA/DSM/IRAMIS/SPCSI, Laboratoire de Chimie des Surfaces et Interfaces, 91191 Gif-sur-Yvette Cedex, France
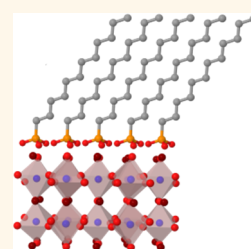
A new step for spintronics would be to benefit from molecular engineering offered by molecules and self-assembled monolayers (SAMs) in particular. Up to now, SAMs have been successfully used to tune the wettability and work function of the metal−organic interface in electronic devices,[1−4] but only two reports have highlighted them as promising for spintronic devices.[5,6] Here, we present results on a building block for molecular/organic spintronics tailoring: the development of the required missing SAM grafting protocols over La$_{2/3}$Sr$_{1/3}$MnO$_3$ (LSMO). LSMO is a highly spin-polarized manganite (nearly one spin direction at the Fermi level), air-stable ferromagnetic oxide,[7,8] which was promoted as one of the most used electrodes[9−12] in organic spintronics.[11,13−17] However, in contrast to the extensive use of chemisorbed SAMs on coinage nonmagnetic metals, proper grafting protocols over LSMO are lacking in the literature and SAMs have yet to be integrated in standard LSMO-based molecular spintronic devices.

Since the first reports on the formation of SAMs, monofunctionalized long alkane chains (C$_n$H$_{2n+1}$X) have proven themselves as one of the preferred and most successful self-assembling units.[18,19] At the end of the chain, thiols and carboxylic and phosphonic acids along with silane groups have commonly been used as molecular anchors.[18−21] In this report, we have tested different combinations of common organic solvents and these monofunctionalized long alkane surfactants for the functionalization of LSMO surfaces.

RESULTS AND DISCUSSION

As a first step toward the functionalization of LSMO surfaces we tested different combinations of common organic solvents (hexane, chloroform, toluene, acetone, ethanol, and tetrahydrofuran) and dodecyl-carboxylic acids (X = −COOH), octadecyl/dodecyl-phosphonic acids (X = −PO$_3$H$_2$), octadecyl-silanes (X = −Si(OCH$_3$)$_3$, −SiCl$_3$), octadecyl-amino (X = −NH$_2$), and octadecyl-thiol (X = −SH). Results are summarized in Table S1.

Only in the case of the alkyl-phosphonic acids were noticeable differences between water advancing contact angle (wCA) values obtained upon immersion of the LSMO substrate in the neat solvent and alkyl-phosphonic solution observed. This fact suggests that only phosphonic acids effectively bind to the LSMO surface[22] and should be the

ABSTRACT (La,Sr)MnO$_3$ manganite (LSMO) has emerged as the standard ferromagnetic electrode in organic spintronic devices due to its highly spin-polarized character and air stability. Whereas organic semiconductors and polymers have been mainly envisaged to propagate spin information, self-assembled monolayers (SAMs) have been overlooked and should be considered as promising materials for molecular engineering of spintronic devices. Surprisingly, up to now the first key step of SAM grafting protocols over LSMO surface thin films is still missing. We report the grafting of dodecyl (C12P) and octadecyl (C18P) phosphonic acids over the LSMO half-metallic oxide. Alkylphosphonic acids form ordered self-assembled monolayers, with the phosphonic group coordinated to the surface and alkyl chains tilted from the surface vertical by 43° (C12P) and 27° (C18P). We have electrically characterized these SAMs in nanodevices and found that they act as tunnel barriers, opening the door toward the integration of alkylphosphonic acid//LSMO SAMs into future molecular/organic spintronic devices such as spin OLEDs.

KEYWORDS: molecular spintronics · self-assembled monolayers · surface functionalization · phosphonic acids · perovskytes · LSMO

Figure 1. AFM images of a C12P LSMO-functionalized surface (24 h, 0.05 mM in ethanol).

TABLE 1. FT-IR Peak Positions for C12P and C18P LSMO-Functionalized Substrates (16 h, 0.05 mM in ethanol)

stretching mode [cm^{-1}]	ν(CH$_3$,a)	ν(CH$_2$,a)	ν(CH$_3$,s)	ν(CH$_2$,s)
C12P	2955	2921	2872	2850
C18P	2958	2922	2869	2852

Figure 2. XPS O1s core level spectrum of a bare LSMO substrate (inset) and a C12P LSMO-functionalized substrate (16 h, 0.05 mM in ethanol).
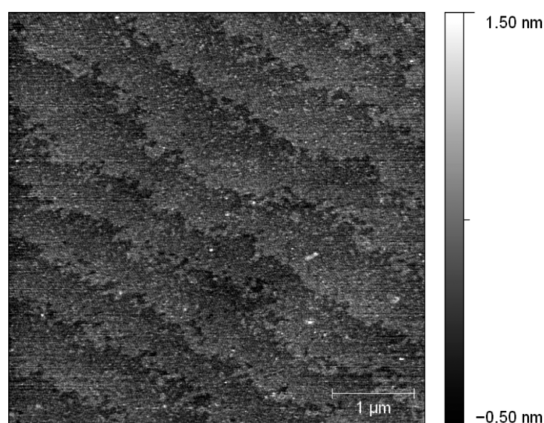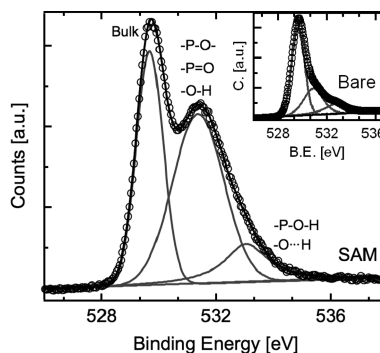
preferred anchoring group for SAM grafting over LSMO. Although all phosphonic acid solutions in polar solvents yielded remarkably high contact angles, the best results were obtained when 0.05 mM ethanolic solutions were used; in that particular case wCAs of 108° and 112° were respectively obtained for dodecyl (C12P) and octadecyl (C18P) phosphonic acids. Grafting from polar solvents is expected to favor stronger tail–tail interactions that will contribute to self-assembly.[23,24] The fact that water contact angle values were unchanged for weeks when the samples were stored under ambient conditions or after successive sonication cycles in different common laboratory solvents underlines the good stability of formed SAMs.

The surface topology of samples deep-casted in 0.05 mM alkylphosphonic acid ethanolic solutions was imaged using atomic force microscopy (AFM) (Figure 1).

No particular differences in surface root-mean-square roughness (about 0.6 nm over 3 μm^2 and <0.3 nm within terraces) or topology were observed between clean and functionalized substrates, and terraces of 500–1000 and 0.5 nm step heights were still observable in the deep-casted substrates. Ellipsometric data were recorded next and analyzed[25] using a Cauchy/triple-amorphous model. Film thicknesses of 12.8 and 22.7 Å were respectively obtained for C12P and C18P, indicating 43° and 27° tilt angles (from the surface normal) for the alkyl chains if they are considered fully stretched. While reasonable, those values are effective values and should be taken with caution considering the presence of substrate terraces (increasing roughness) and potential SAM disorder (higher for C18P, see below). Next, Fourier transform infrared spectra of the C12P- and C18P-functionalized substrates were carried out. Analysis of the signals associated with the P–O–(H) was hampered by the strong absorption of both LSMO and STO between 1400 and 600 cm^{-1}, and we were able to analyze only the aliphatic region between 3100 and 2700 cm^{-1}. The observed peak positions associated with the different

CH$_2$ and CH$_3$ groups are displayed in Table 1 and Figure S1.

Comparing the vibration wavenumbers associated with the different CH$_2$ and CH$_3$ groups allows us to see a shift to higher wavenumbers in C18P's vibrational modes when compared with those of C12P and may indicate a decreased order in the case of the C18P.[22] The CH$_2$/CH$_3$ intensity ratio (Figure S2) is proportionally higher than those observed in bulk C12P and C18P spectra, as expected for tilted alkylic chains.[26]

Next, we studied the C12P and C18P SAMs using X-ray photoelectron spectroscopy (XPS). XPS spectra clearly showed the presence of the P2s and P2p peak (partially masked by the Sr3d peak) associated with the phosphonic acid group, further denoting the presence of the monolayer (Figure S3). The high-resolution O1s core level spectrum shown in Figure 2 could be deconvoluted into three peaks and assigned to different oxygen species:[27–30] –P–O–H groups, adsorbed water, and loosely bond oxygen species (533.1 eV), surface hydroxides, –P–O–, and/or –P=O (531.4 eV), and bulk LSMO oxygen (529.7 eV).

The comparison of obtained peak ratio (1.0/0.9/0.6) with that obtained in the case of bare LSMO substrates (1.0/0.4/0.8) suggests that the presence of unbound –P–O–H groups is not significant (Figure 2) and phosphonic acid groups are mainly bound to the surface in a bidentate and/or tridentate mode. Summarizing, wCA ellipsometric, FT-IR, and XPS data support the formation of a stable and ordered SAM of alkylphosphonic acids over LSMO in which the C12P and C18P alkyl chains are fully stretched and approximately 43° and 27° deviated from the surface vertical and bonded to the surface in a bidentate and/or tridentate mode (Figure 3).

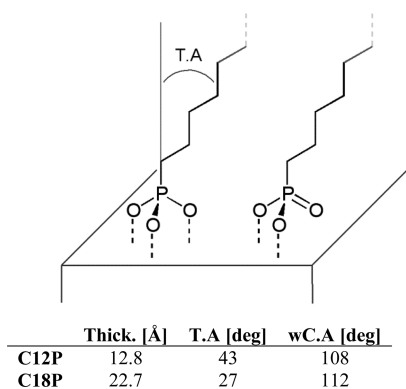|	Thick. [Å]	T.A [deg]	wC.A [deg]
C12P	12.8	43	108
C18P	22.7	27	112

Figure 3. Proposed structure for alkylphosphonic SAMs over LSMO (top). C12P and C18P measured thickness, tilt angle (TA), and water advancing contact angle (wCA) (bottom).
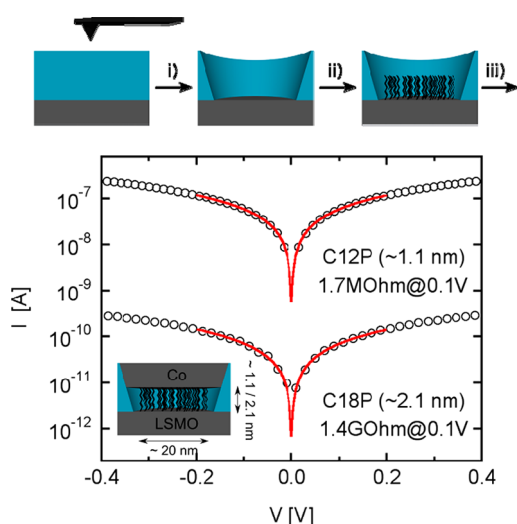

Figure 4. Basic steps of the indentation process (top). Representative semilog plots of the $I(V)$ traces (dots) of Co/C12P//LSMO and Co/C18P//LSMO junctions. Tunnelling characteristic fit (see text) up to 0.2 V (line).

Once the missing protocol for the alkylphosphonic acid functionalization of LSMO surfaces had been developed, we have checked the tunnelling behavior of these SAMs grafted on LSMO by contacting them in between nanometric size electrodes (approximately 20 nm section) by following previously described procedures.[31]

Figure 4 schematically describes the steps followed for SAM nanocontacting. Briefly, an AFM tip was used to notch holes on a resist previously deposited on the conductive substrate (i). Then the exposed surface through the opened hole was SAM functionalized (ii). Finally, the top contact was deposited (iii).

In Figure 4 we also show local $I(V)$ curves recorded at room temperature on these nanocontacs. In order to highlight the tunnelling behavior of our devices, we performed $I(V)$ curve fits following the work by Akkerman et al.[32] (based on the model introduced by Simmons[33] with the image potential included). We used a dielectric constant of the monolayer (ε_r)
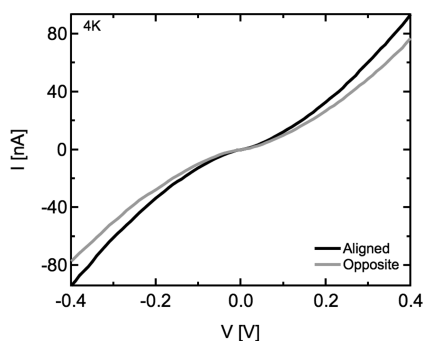

Figure 5. Representative $I(V)$ traces at $T = 4$ K of Co/C12P//LSMO junctions in the aligned (black) and opposite (gray) magnetic configurations.

of 2.1 and an effective mass (α) of 0.28 for the alkyl chain, which gave mean barrier heights in the 1.5–2.5 eV range (corresponding to a nominal barrier height without image potential (Φ) of around 3.5 eV). To compare with previous studies, we also tentatively provide an estimation of the convenient parameter β (the tunnelling decay coefficient) associated with the exponential decrease of tunnelling current with chain length. For monosubstituted alkyl chains, β values are usually found in the range 0.6 to 0.9 Å^{-1}, depending on the measurement technique, contact area, binding group, or electrodes.[34,35] Here, from the $I(V)$ curves we could roughly estimate a tunnelling decay coefficient $\beta = \sqrt{(\alpha\Phi_{mean})}$ in the 0.65–0.84 Å^{-1} range. This range is also in agreement with the observed increase in contact resistance with molecular length ($\propto \exp(\beta d)$).[34,35]

If SAMs have to be used in spintronic devices, it is important that their grafting will not affect the electrode spin polarization properties. In order to prove that electrode spin polarization is kept after alkyl phosphonic acid grafting, we follow an analogy to aligned and cross optical polarizers/analyzers. We performed transport measurement in aligned and opposite spin polarization configurations. The two configurations were obtained by successively applying a high magnetic field (+0.4 T) to saturate both electrodes' magnetizations in the same direction and then reversing the field to a small negative value (−80 mT) to switch back only the LSMO magnetization. As is shown in Figure 5, a difference in device conductivity is observed between both configurations. This is a direct demonstration that the LSMO surface is still spin polarized after the grafting and lithography process and that spin-polarized transport through akyl-phosphonic SAMs is possible. This clearly highlights the potential of alkylphosphonic SAMs on LSMO in the development of future molecular spintronic devices.

CONCLUSIONS

In conclusion, we have presented results on a building block for molecular spintronics tailoring: the development of the required missing SAM grafting protocols over the commonly used LSMO ferromagnetic electrode.

We have shown that alkylphosphonic acid groups should be envisaged as the preferred anchoring group when dealing with the self-assembled monolayer functionalization of the standard ferromagnetic electrode material LSMO. Furthermore, we have demonstrated that C12P and C18P monolayers grafted on LSMO act as tunnel barriers. We have analyzed the obtained results using Simmons' model and found that the parameters describing our system are close to those reported previously for alkanethiols and akylphosphonates with similar carbon chains lengths. Finally, we have shown that LSMO electrodes do not lose their spin polarization after the grafting process. Our results open the door to the integration of alkylphosphonic chains into spintronic devices.

EXPERIMENTAL PROCEDURES

LSMO substrates were elaborated by pulsed laser deposition on double-polished $SrTiO_3$ (STO) substrates. The LSMO nominal thickness was around 25 nm, as determined by spectroscopic ellipsometry and X-ray reflectometry. Top electrodes were deposited by sputtering. Immediately before SAM functionalization, substrates were sonicated for 5 min cycles in acetone, trichloroethane, 2-propanol, and water and were dried under a stream of nitrogen. Next, they were treated for 120 s with a 15 W oxygen plasma.

SAMs were prepared by immersion of the LSMO substrates into 2 mL of a freshly filtered 5 to 0.05 mM solution of the corresponding surfactant dissolved in the desired organic solvent. After 1−3 days of immersion wafers were removed from the solution and rinsed thoroughly with neat solvent. All the functionalization experiments were carried out at room temperature.

Contact angles of the different LSMO substrates were measured in air with deionized water. Images of the substrates were obtained in intermittent contact mode. For imaging we used Si cantilevers with a nominal spring constant of 40 N/m, a tip radius of curvature of less than 5 nm, and a resonant frequency of 300 kHz. For the construction of the nanocontacts an insulating Shipley S1805 positive photoresist layer approximately 40 nm thick was deposited over the LSMO substrates. The thickness of the resist was adjusted by diluting the S1805 resist with Shipley EC solvent. A hard-bake step was used to adjust the resist's mechanical properties and to allow subsequent photolithographic processes without damaging the resist layer. AFM 40 N/m diamond tips were then used to notch the holes into the resist. An additional oxygen plasma treatment may have been used to enlarge the size of the holes. SAMs were then deposited, and the top contact electrodes were finally deposited by sputtering. Ellipsometric data were in the 270−700 nm spectral range in 5 nm steps at an angle of incidence of 70°. Substrate−monolayer data were fitted to a double-slab model. Here, the STO substrate and LSMO thin films were modeled with a new triple amorphous dispersion law,[36,37] and SAM was modeled with a Cauchy dispersion law[38] (the diffraction index (n) of the SAM was fixed to 1.49).[22] Experimental uncertainty in the thickness is estimated at ±2 Å. Thicknesses were estimated as the distance between the terminal oxygen and the methyl hydrogen in a fully stretched chain. All bond angles were considered to be 109.5°, and bond distances were taken to be O−P = 1.55, P−C = 1.78,[39] C−C = 1.54, and C−H = 1.10 Å.[40] The thickness can then be approximated as $T \approx 0.82(4.42 + (n − 1)1.54)$, where n is the number of carbons in the chain. Substrates with the SAM were placed (face down) between the Ge crystal and the tip of the high-pressure clamp. Each FTIR spectrum represents the average of at least 128 scans at 4 cm^{-1} resolution. The infrared beam was p-polarized by means of a manual ZnSe polarizer, and the output signal was collected with a refrigerated mercury cadmium telluride detector. X-ray photoelectron spectroscopy was carried out using monochromated Al Kα X-rays ($h\nu$ = 1486.6 eV), a hemispherical analyzer, and a channel plate detector. The spectrometer was calibrated at the Au 4f core level at a binding energy of 84 eV. Spectra were recorded at a takeoff angle of 90°. The pass energy was set to 160 eV for survey and 20 eV for core level, giving an energy resolution of 0.38 eV.

Conflict of Interest: The authors declare no competing financial interest.

REFERENCES AND NOTES

1. Dibenedetto, S. A.; Facchetti, A.; Ratner, M. A.; Marks, T. J. Molecular Self-Assembled Monolayers and Multilayers for Organic and Unconventional Inorganic Thin-Film Transistor Applications. *Adv. Mater.* **2009**, *21*, 1407–1433.

2. Braun, S.; Salaneck, W.; Fahlman, M. Energy-Level Alignment at Organic/Metal and Organic/Organic Interfaces. *Adv. Mater.* **2009**, *21*, 1450–1472.

3. Tsao, H. N.; Müllen, K. Improving Polymer Transistor Performance via Morphology Control. *Chem. Soc. Rev.* **2010**, *39*, 2372.

4. Halik, M.; Hirsch, A. The Potential of Molecular Self-Assembled Monolayers in Organic Electronic Devices. *Adv. Mater.* **2011**, *23*, 2689–2695.

5. Petta, J.; Slater, S.; Ralph, D. Spin-Dependent Transport in Molecular Tunnel Junctions. *Phys. Rev. Lett.* **2004**, *93*, 136601.

6. Wang, W.; Richter, C. Spin-Polarized Inelastic Electron Tunneling Spectroscopy of a Molecular Magnetic Tunnel Junction. *Appl. Phys. Lett.* **2006**, *89*, 153105.

7. Mercone, S.; Perroni, C.; Cataudella, V.; Adamo, C.; Angeloni, M.; Aruta, C.; de Filippis, G.; Miletto, F.; Oropallo, A.; Perna, P.; *et al.* Transport Properties in Manganite Thin Films. *Phys. Rev. B* **2005**, *71*, 064415.

8. Bowen, M.; Maurice, J.-L.; Barthélémy, A.; Bibes, M.; Imhoff, D.; Bellini, V.; Bertacco, R.; Wortmann, D.; Seneor, P.; Jacquet, E.; *et al.* Using Half-Metallic Manganite Interfaces to Reveal Insights Into Spintronics. *J. Phys.: Condens. Matter* **2007**, *19*, 315208.

9. Dediu, V.; Murgia, M.; Matacotta, F.; Taliani, C.; Barbanera, S. Room Temperature Spin Polarized Injection in Organic Semiconductor. *Solid State Commun.* **2002**, *122*, 181–184.

10. Xiong, Z. H.; Wu, D.; Vardeny, Z. V.; Shi, J. Giant Magnetoresistance in Organic Spin-Valves. *Nature* **2004**, *427*, 821–824.

11. Dediu, V.; Hueso, L.; Bergenti, I.; Taliani, C. Spin Routes in Organic Semiconductors. *Nat. Mater.* **2009**, *8*, 707–716.

12. Barraud, C.; Seneor, P.; Mattana, R.; Fusil, S.; Bouzehouane, K.; Deranlot, C.; Graziosi, P.; Hueso, L.; Bergenti, I.; Dediu, V.; *et al.* Unravelling the Role of the Interface for Spin Injection into Organic Semiconductors. *Nat. Phys.* **2010**, *6*, 615–620.

13. Camarero, J.; Coronado, E. Molecular vs. Inorganic Spintronics: the Role of Molecular Materials and Single Molecules. *J. Mater. Chem.* **2009**, *19*, 1678–1684.

14. Wang, F.; Vardeny, Z. V. Recent Advances in Organic Spin-Valve Devices. *Synth. Met.* **2010**, *160*, 210–215.

15. Sanvito, S. Molecular Spintronics. *Chem. Soc. Rev.* **2011**, *40*, 3336–3355.

16. Shiraishi, M.; Ikoma, T. Molecular Spintronics. *Phys. E (Amsterdam, Neth.)* **2011**, *43*, 1295–1317.

17. Szulczewski, G. J. Spin Polarized Electron Tunneling and Magnetoresistance in Molecular Junctions. *Top. Curr. Chem.* **2011**, *312*, 275–302.

18. Ulman, A. Formation and Structure of Self-Assembled Monolayers. *Chem. Rev.* **1996**, *96*, 1533–1554.

19. Schreiber, F. Structure and Growth of Self-Assembling Monolayers. *Prog. Surf. Sci.* **2000**, *65*, 151–256.

20. Kind, M.; Wöll, C. Organic Surfaces Exposed by Self-Assembled Organothiol Monolayers: Preparation, Characterization, and Application. *Prog. Surf. Sci.* **2009**, *84*, 230–278.

21. Queffélec, C.; Petit, M.; Janvier, P.; Knight, D. A.; Bujoli, B. Surface Modification Using Phosphonic Acids and Esters. *Chem. Rev.* **2012**, *112*, 3777–3807.

22. Ulman, A. *An Introduction to Ultrathin Organic Films: From Langmuir-Blodgett to Self-Assembly*; Academic Press, 1991.

23. Nie, H.; Walzak, M.; McIntyre, N. Delivering Octadecylphosphonic Acid Self-Assembled Monolayers on a Si Wafer and Other Oxide Surfaces. *J. Phys. Chem. B* **2006**, *110*, 21101–21108.

24. Ito, Y.; Virkar, A. A.; Mannsfeld, S.; Oh, J. H.; Toney, M.; Locklin, J.; Bao, Z. Crystalline Ultrasmooth Self-Assembled Monolayers of Alkylsilanes for Organic Field-Effect Transistors. *J. Am. Chem. Soc.* **2009**, *131*, 9396–9404.

25. Tompkins, H. G.; McGahan, W. A. *Spectroscopic Ellipsometry and Reflectometry: A User's Guide*; John Wiley & Sons, Inc., 1999.

26. Tillman, N.; Ulman, A.; Schildkraut, J.; Penner, T. Incorporation of Phenoxy Groups in Self-Assembled Monolayers of Trichlorosilane Derivatives: Effects on Film Thickness, Wettability, and Molecular Orientation. *J. Am. Chem. Soc.* **1988**, *110*, 6136–6144.

27. Liang, J.-J.; Weng, H.-S. Catalytic Properties of $La_{1-x}Sr_xBo_3$ (B = Mn, Fe, Co, Ni) for Toluene Oxidation. *Ind. Eng. Chem. Res.* **1993**, *32*, 2563–2572.

28. Rao, W.; Yu, J. The Structural and Morphology of $(La_{0.7}Sr_{0.3})MnO_3$ Thin Films Prepared by Pulsed Laser Deposition. *Adv. Mater. Res.* **2011**, *150−151*, 908–911.

29. Textor, M.; Ruiz, L.; Hofer, R.; Rossi, A.; Feldman, K.; Hähner, G.; Spencer, N. D. Structural Chemistry of Self-Assembled Monolayers of Octadecylphosphoric Acid on Tantalum Oxide Surfaces. *Langmuir* **2000**, *16*, 3257–3271.

30. Zorn, G.; Gotman, I.; Gutmanas, E. Y.; Adadi, R.; Salitra, G.; Sukenik, C. N. Surface Modification of Ti45Nb Alloy with an Alkylphosphonic Acid Self-Assembled Monolayer. *Chem. Mater.* **2005**, *17*, 4218–4226.

31. Bouzehouane, K.; Fusil, S.; Bibes, M.; Carrey, J.; Blon, T.; Le Dû, M.; Seneor, P.; Cros, V.; Vila, L. Nanolithography Based on Real-Time Electrically Controlled Indentation with an Atomic Force Microscope for Nanocontact Elaboration. *Nano Lett.* **2003**, *3*, 1599–1602.

32. Akkerman, H.; Naber, R.; Jongbloed, B.; van Hal, P.; Blom, P.; de Leeuw, D.; de Boer, B. Electron Tunneling Through Alkanedithiol Self-Assembled Monolayers in Large-Area Molecular Junctions. *Proc. Natl. Acad. Sci. U. S. A.* **2007**, *104*, 11161–11166.

33. Simmons, J. G. Generalized Formula for the Electric Tunnel Effect Between Similar Electrodes Separated by a Thin Insulating Film. *J. Appl. Phys.* **1963**, *34*, 1793–1803.

34. Salomon, A.; Cahen, D.; Lindsay, S.; Tomfohr, J.; Engelkes, V. B.; Frisbie, C. D. Comparison of Electronic Transport Measurements on Organic Molecules. *Adv. Mater.* **2003**, *15*, 1881–1890.

35. Wang, W.; Lee, T.; Reed, M. A. Electron Tunnelling in Self-Assembled Monolayers. *Rep. Prog. Phys.* **2005**, *68*, 523–544.

36. He, G.; Zhang, L.; Li, G.; Liu, M.; Wang, X. Structure, Composition and Evolution of Dispersive Optical Constants of Sputtered TiO_2 Thin Films: Effects of Nitrogen Doping. *J. Phys. D* **2008**, *41*, 045304.

37. Kim, J.-E.; Bae, S.-M.; Yang, H.-S.; Hwang, J.-H. Electrical and Optical Properties of Zinc Oxide Thin Films Deposited Using Atomic Layer Deposition. *J. Kor. Ceram. Soc.* **2010**, *47*, 353–356.

38. *Handbook of Ellipsometry*; Tompkins, H. G.; Eugene, I. A., Eds.; William Andrew Inc., 2005.

39. Mahmoudkhani, A.; Langer, V. Supramolecular Isomerism and Isomorphism in the Structures of 1,4-Butanebisphosphonic Acid and Its Organic Ammonium Salts. *Cryst. Growth Des.* **2002**, *2*, 21–25.

40. *Handbook of Chemistry and Physics*; Weast, C., Ed.; The Chemical Rubber Co., 1970.